Quasielastic Light-Scattering Study of Semiflexible Polymers. Poly(γ-benzyl L-glutamate) in Dimethylformamide

Kenji Kubota* and Yasunori Tominaga

Department of Physics, Faculty of Science, Ochanomizu University, Bunkyo-ku, Tokyo 112, Japan

Satoru Fujime

Mitsubishi-Kasei Institute of Life Sciences, Machida, Tokyo 194, Japan.
Received October 30, 1985

ABSTRACT: Quasielastic light-scattering measurements are made for dilute solutions of semiflexible polymers, poly(γ-benzyl L-glutamate), of molecular weights 3×10^5 and 3.7×10^5 in dimethylformamide, with particular emphasis on the internal bending motion. Experimental intensity autocorrelation functions are analyzed by a modified two-exponential fit and by a cumulant expansion. The translational and rotational diffusion coefficients thus obtained are compared with predicted values from recent theories, and fairly good agreement is obtained. The observed $\bar{\Gamma}/K^2$ vs. K^2 relationship is analyzed by use of a theoretical formulation including anisotropy in translational diffusion, chain flexibility, and the hydrodynamic interaction (Maeda, T.; Fujime, S. *Macromolecules* **1984**, *17*, 2381), where $\bar{\Gamma}$ is the first cumulant of the field correlation function and K is the length of the scattering vector. Results suggest the important contributions to $\bar{\Gamma}/K^2$ from anisotropy in translational diffusion and from chain flexibility, and the above theory with a recently reevaluated value of the persistence length of this polymer in a helicogenic solvent can account for the behavior of $\bar{\Gamma}/K^2$ against K^2 quantitatively.

Introduction

Quasielastic light scattering has been extensively applied to the study of dynamic properties of macromolecules in solutions and has been proven to be a useful tool for such study.[1,2] Recently, it has been applied to much more complicated systems such as entangled, semidilute, and concentrated solutions or melt systems.[3] Not only synthetic macromolecular systems but also micellar and biological systems have been studied, and very useful information about dynamical characterization is extracted.[4]

In most cases up to now, however, the objective polymers have been flexible coils, polystyrene, for example, and only a few studies of rodlike and semiflexible polymer systems have been carried out. To understand the experimental spectrum (or the time correlation function) of light scattered from solutions of long and semiflexible polymers, theoretical models for rigid rods undergoing translational and rotational Brownian motions are usually applied as a first-order approximation. Because a geometrically anisotropic particle such as a long rod undergoes anisotropic translation, a coupling between translational and rotational modes of diffusive motions is expected.[5] This effect has been studied experimentally in detail with special reference to tobacco mosaic virus, and the strong effect of anisotropic translation on the the field correlation function has become clear.[6,7]

Even if rods seem (or are believed) to be rigid, they might be semiflexible when they are very long. Even in the static light-scattering experiments, the profile of the scattering intensity reveals clearly a deviation from rigid-rod behavior, and an explicit inclusion of flexibility into the theoretical formulation is essential.[8] The flexion motion of long rods contributes to the spectrum of light.[9] The characterization, then, of the flexion motion is quite important. Maeda and Fujime examined this problem theoretically[10,11] and experimentally by using monodisperse suspensions of fd virus.[12] In their study, a reasonable value of γL (=0.23) is obtained, where γ is the flexibility parameter of the filament. This γL value is very close to that obtained from a statistical analysis of virus images on electron micrographs. This suggests that the formulation for the field correlation function, including anisotropy in translation, filament flexibility, and the hydrodynamic interaction, is reasonable and provides a practical procedure to estimate the filament flexibility.

Some polypeptides take an α-helical structure under certain conditions and behave as rodlike molecules. Among them, poly(γ-benzyl L-glutamate) (PBLG) is one of the most frequently investigated polymers. PBLG molecules are usually studied as a model material of a rod. But PBLG in helicogenic solvent begins to gain some degree of flexibility as the molecular weight increases and has been treated by a wormlike chain model of Kratky and Porod.[13] Previously, Kubota and Chu studied quasielastic light scattering of PBLG in dimethylformamide (DMF), which is one of typical helicogenic solvents of PBLG, mainly focusing on the examination of the dynamical behavior in a semidilute region.[14] They examined also the K^2 dependence of $\bar{\Gamma}/K^2$ in terms of the Maeda and Fujime theory,[9] where $\bar{\Gamma}$ is the first cumulant or the average decay rate of the field correlation function. In that study, the rotational diffusion coefficient was determined at one high angle (135°) with a histogram analysis of the decay rate distribution by imposing a bimodal distribution and by ignoring higher modes. But, as was observed in the study of tobacco mosaic virus,[7] higher order modes with even smaller amplitudes contribute substantially to the correlation function and cause to increase the magnitude of the decay rate of the fast component. In such a case, the analysis of the K^2 dependence of $\bar{\Gamma}/K^2$ is necessary, and the large value of the rotational diffusion coefficient in that study[14] is opened for reevaluation. Furthermore, the assignment of the $n = 1$ mode of the flexion motion in the Maeda and Fujime theory to the rotational Brownian motion is not exactly correct, especially at relatively low γL.[9] The K^2 dependence of $\bar{\Gamma}/K^2$ should then be examined in a more detailed manner based on more sophisticated theoretical treatments. One of the purposes of the present work is to study this point in detail.

Yamakawa is one of the pioneers who studied the characterization of semiflexible polymers and has obtained many valuable results on the basis of the wormlike chain model.[15,16] Recently, he extended a wormlike chain model to a helical wormlike chain model, including the torsional rigidity, and obtained useful knowledge about static and dynamic statistical properties of polymers.[17,18] For PBLG

0024-9297/86/2219-1604$01.50/0

in DMF, he evaluated γ^{-1} = 313 nm or the persistence length of 156.$_5$ nm by using the data of Fujita et al.[19] and others.[20] This value is quite larger than previously used. It should be examined whether this value of the persistence length predicts well the light-scattering spectrum.

Schmidt and Stockmayer examined the quasielastic light-scattering spectrum at low K^2 theoretically for several models for a semiflexible chain[21] and discussed the C parameter[22] in the K^2 dependence of $\bar{\Gamma}/K^2$. Schmidt examined the effect of polydispersity on the spectrum of PBLG in DMF by combining static and quasielastic light-scattering experiments[23] and showed that the neglect of polydispersity led to an underestimation of chain flexibility. He obtained quite a low value of γ^{-1}.

In the present work, the K^2 dependence of the first cumulant of the field correlation function for PBLG, of molecular weights 3×10^5 and 3.7×10^5 in DMF at a dilute solution region, is investigated to examine the effect of flexibility on the light-scattering spectrum, and comparison of experimental results with predictions of a theory including filament flexibility, anisotropy in translation, and the hydrodynamic interaction is carried out mainly with the aid of a recent theory of Fujime and Maeda.[10,11]

Theoretical Background

1. Quasielastic Light Scattering. a. Rigid Rods. The position vector $\mathbf{r}(s,t)$, relative to the laboratory-fixed coordinate origin, of the line element ds at s on the rod with length L is defined by

$$\mathbf{r}(s,t) = \mathbf{R}(t) + s\mathbf{t}(t) \tag{1}$$

where $\mathbf{R}(t)$ is the position vector, relative to the laboratory-fixed origin, of the center of resistance of the rod, $\mathbf{t}(t)$ is the unit vector parallel to the rod axis, and t is time.[24] The field correlation function of polarized scattered light is given by

$$G^1(\tau) = (1/L^2)\int\int_{-L/2}^{L/2} J(s,s',\tau)\, ds\, ds' \tag{2}$$

$$J(s,s',\tau) = \langle \exp[i\mathbf{K}\{\mathbf{r}(s,t) - \mathbf{r}(s',t')\}]\rangle \tag{3}$$

where $\tau = |t - t'|$ and $\langle ... \rangle$ denotes the statistical average. The Brownian motion of $\mathbf{R}(t)$ and $\mathbf{t}(t)$ can be described by the translational/rotational diffusion equation. $G_K(\xi,\xi';\tau) = G_D(\tau)g_K(\xi,\xi';\tau)$ denotes the Fourier space transform of the Green function to the diffusion equation, where

$$G_D(\tau) = \exp[-\{D_0 - (1/3)(D_3 - D_1)\}K^2\tau] \tag{4}$$

In eq 4, D_0 is the overall, D_3 is the lengthways, and D_1 is the sideways translational diffusion coefficient. Then, we have from eq 1 and 3

$$J(s,s',\tau) = G_D(\tau)(1/2)\int\int_{-1}^{1} e^{iK(s\xi - s'\xi')} g_K(\xi,\xi';\tau)\, d\xi\, d\xi' \tag{5}$$

where $\xi = \cos\theta(t)$ and $\xi' = \cos\theta(t')$, $\theta(t)$ being the instantaneous angle between $\mathbf{t}(t)$ and $\mathbf{K}$, the scattering vector in the laboratory-fixed coordinate system. The explicit form of $g_K(\xi,\xi';\tau)$ has been given elsewhere.[24] By definition, the first cumulant $\bar{\Gamma}$ of $G^1(\tau)$ is given by $\bar{\Gamma} = -\lim (\partial/\partial\tau) \ln G^1(\tau)$, where "lim" means to take the limiting value at $\tau = 0$ of its operand. Then, from eq 2, 4, and 5, we have

$$\bar{\Gamma}/K^2 = [D_0 - (1/3)(D_3 - D_1)] + (L^2/12)\Theta f_1(k) + (D_3 - D_1)f_2(k) \tag{6}$$

where Θ is the end-over-end rotational diffusion coefficient of the rod and $f_1(k)$ and $f_2(k)$ are functions depending only on $k = KL/2$ (see the last part in 1b). This formulation was discussed previously and thoroughly examined experimentally by use of suspensions of tobacco mosaic virus.[6,7] The validity of eq 6 was ascertained, and the importance of the coupling between translational and rotational diffusion, due to anisotropy in translation, has become clear.

b. Semiflexible Filaments. A simple extension of eq 1 gives

$$\mathbf{r}(s,t) = \mathbf{R}(t) + s\mathbf{t}(t) + \sum_{n\geq 2} \mathbf{q}(n,t)Q(n,s) \tag{7}$$

where terms $\mathbf{q}(n,t)Q(n,s)$ come from the flexion motion of the filament. From eq 3 and 7, we have (cf. eq 5)

$$J(s,s',\tau) = G_D(\tau)(1/2)\int\int e^{iK(s\xi - s'\xi')} g_K(\xi,\xi';\tau) \times \prod_{n\geq 2} \exp[-\Phi(n,s,s',\xi,\xi',\tau)]\, d\xi\, d\xi' \tag{8}$$

where the internal factor $\Phi(...)$ is given elsewhere.[10] The above expression of $G^1(\tau)$ is quite complicated, but the first cumulant has a simple form (cf. eq 6)

$$\bar{\Gamma}/K^2 = [D_0 - (1/3)(D_3 - D_1)] + (L^2/12)\Theta f_1^*(k) + (D_3 - D_1)f_2^*(k) + (k_BT/\zeta L)\sum_{n\geq 2}(1 + f_n)a_n(k) \tag{9}$$

where ζ ($=4\pi\eta$) is the friction constant per unit length,[11] L is the contour length of the semiflexible filament, k_B is the Boltzmann constant, T is the absolute temperature, and f_n is given later. By defining

$$\Psi(s,s',\xi,\xi',\tau) = e^{iK(s\xi - s'\xi')} \prod_{n\geq 2} e^{-\Phi(n,s,s',\xi,\xi',\tau)} \tag{10}$$

we have[10]

$$f_1^*(k) = (3/k^2)\sum_n n(n+1)(2n+1)I_{n,n}/G^1(0) \tag{11}$$

$$f_2^*(k) = \sum_n [(2n+1)L_0(n)I_{n,n} + (2n-3)L_1(n)I_{n,n-2} + (2n+5)L_2(n)I_{n,n+2}]/G^1(0) \tag{12}$$

$$a_n(k) = [1/2LG^1(0)]\int d\xi' \int\int ds\, ds' (1 - \xi'^2)Q(n,s)Q(n,s')\Psi(s,s',\xi,\xi',0) \tag{13}$$

$$I_{n,m} = (1/4L^2)\int\int d\xi\, d\xi' \int\int ds\, ds' \times P_n(\xi)P_m(\xi')\Psi(s,s',\xi,\xi',0) \tag{14}$$

$$G^1(0) = (1/2L^2)\int d\xi' \int\int \Psi(s,s',\xi,\xi',0)\, ds\, ds' \tag{15}$$

where $L_i(n)$ (i = 0, 1, and 2) are simple functions of integer n (ref 24) and $P_n(\xi)$ is the nth-order Legendre polynomial. Equations 11–15 are functions of not only k but also γL through γL dependence of $\Phi(n,s,...)$.

The spherically averaged hydrodynamic interaction tensor is given by $H(s,s') = \delta(s - s') + (\zeta/6\pi\eta)f(|s - s'|)$, where ζ ($=3\pi\eta$) is the spherically averaged friction constant[11] and the function $f(|s - s'|)$ has been discussed by Hearst and Stockmayer.[25] From this form of $H(s,s')$, f_n in eq 9 is given by[11]

$$f_n = (1/2)\int\int Q(n,s)f(|s - s'|)Q(n,s')\, ds\, ds' \tag{16}$$

Eigenfunctions $Q(n,s)$ and eigenvalues λ_n are given elsewhere,[10] so that explicit computation of $f_1^*(k)$, $f_2^*(k)$, $a_n(k)$, and f_n is possible. However, the machine computation of $I_{n,m}$ in eq 14 is very time consuming because of 4-fold integration and is not practical. As previously shown,[10] however, ξ in $\Phi(...)$ can be replaced with ξ' with very high accuracy. Then, eq 14 can be approximated as

$$I_{n,m} = (i^n/2L^2)\int d\xi' \int\int ds\, ds'\, j_n(Ks)P_m(\xi')e^{-iKs'\xi'} \times \prod_{l\geq 2} \exp[-\Phi(l,s,s',\xi',\xi',0)] \tag{14'}$$

where $j_n(Ks)$ is the nth-order spherical Bessel function.

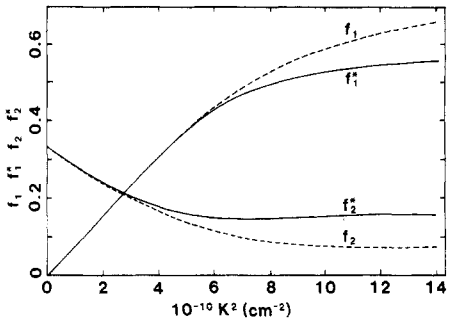

Figure 1. Graphic representation of $f_1^*(k)$, $f_2^*(k)$, $f_1(k)$, and $f_2(k)$ as functions of K^2 for L = 255 nm (PBLG-B). $f_1^*(k)$ and $f_2^*(k)$ are for a semiflexible chain with γ^{-1} = 313 nm, and $f_1(k)$ and $f_2(k)$ are for a rigid rod.

For a rigid rod ($\gamma L = 0$), we have $I_{n,m} = (i)^n(-i)^m b_n(k)b_m(k)$ and $G^1(0) = \sum_n (2n+1)b_n(k)^2$, where $b_n(k)$ is the dynamic form factor for a rigid rod. Then, we have $f_1^*(k) \to f_1(k)$ and $f_2^*(k) \to f_2(k)$. In this limit, $a_n(k)$ should be zero, but $a_n(k)$ in eq 13 has a finite value. This comes from the fact that $\langle q(n,t)^2\rangle \to 0$ and τ_n (the relaxation time of the nth mode) $\to 0$, *but* $\langle q(n,t)^2\rangle/\tau_n \to$ finite as $\gamma L \to 0$.[9,26] As shown later, however, this trouble is not serious for at least $a_2(k)$. The computed $f_1^*(k)$ and $f_2^*(k)$ for γ^{-1} = 313 nm and L = 255 nm are shown in Figure 1 with $f_1(k)$ and $f_2(k)$ for a rigid rod with L = 255 nm.

2. Diffusion Coefficients. a. Rigid Rods. For a rigid rod with length L and diameter d, diffusion coefficients D_1, D_3, $D_0 = (2D_1 + D_3)/3$ and Θ can be computed by use of Broersma's[27,28] or Tirado and Garcia de la Torre's[29] formulas.

b. Semiflexible Filaments. Diffusion coefficients of the semiflexible filaments with the contour length L and diameter d should be functions of γL; Yamakawa and Fujii[16] gave a formula for D_0 and Yoshizaki and Yamakawa[17] and Hagerman and Zimm[30] gave formulas for Θ. The latter two theories gave Θ values very close to each other, although the basic starting ideas are quite different from each other. No detailed theory for D_1 and D_3 is presented up to now. Schmidt and Stockmayer gave an approximate formula[21]

$$(D_3 - D_1)/D_0 = (3/4)[1 - 0.5(\gamma L)^{1/4}] \qquad (17)$$

where the factor (3/4) is the value in the long-rod limit. An alternative value may be given by use of Broersma's or Garcia de la Torre's formulas.

3. $\bar{\Gamma}/K^2$ vs. K^2 in the Low K^2 Limit. At low K^2, $\bar{\Gamma}/K^2$ can be given by $\bar{\Gamma}/K^2 = D_0[1 + C\langle r_g^2\rangle K^2 + ...]$, where C is a constant depending on chain stiffness, polydispersity, and chain structure,[22] and $\langle r_g^2\rangle$ is the mean square radius of gyration. If we use experimental values of $\bar{\Gamma}(c)$, $D_0(c)$, and $\langle r_g(c)^2\rangle_z$ at concentration c, we have

$$\bar{\Gamma}(c)/K^2 = D_0(c)[1 + C\langle r_g(c)^2\rangle_z K^2 + ...] \qquad (18)$$

The parameter C determined from eq 18 would be less dependent on c.

Experimental Section

1. Sample Preparation. The PBLG sample was kindly provided by Professor K. Ogino of the University of Tokyo. The original PBLG sample was fractionated by successive precipitation fractionation by using DMF as a solvent and methanol as a precipitant. Seven fractions were obtained, and two of them (PBLG-A and -B) were used in the experiments. PBLG samples were vacuum-dried just before they were dissolved in DMF. DMF was dried over molecular sieves and fractionally distilled before use. The concentration of the solution was determined gravimetrically. The solution was filtered through a Teflon filter with 1-μm pore size directly into a 10-mm-o.d. polished cylindrical glass cell, which had been washed thoroughly with filtered benzene (with 0.2-μm pore size) and dried under dust-free circumstances. The solution in the sample cell was centrifuged at ca. 10000g for 1 h just before measurements in order to keep the remaining dust particles off the scattering volume.

2. Light-Scattering Spectrometer. The light-scattering measurements were carried out with a homemade spectrometer and a 252-channel real-time correlator. The details of this system are described elsewhere.[7] One thing to be added is that calibration was done by taking the Rayleigh ratio R_{vv} of benzene at 25 °C and 488.0 nm to be 32.0×10^{-6} cm^{-1}.[31]

The correlator equipped two types of circuits to independently determine the base line of the correlation function.[7] The base lines determined by use of these two circuits agreed with each other within 0.1%, verifying the optical purification of the scattering sample.

3. Data Analysis. The angular dependence of the absolute static intensity as a function of the polymer concentration c (g/cm^3) is related to the weight-average molecular weight M_w, the scattering function $P(K)$ and the second virial coefficient A_2 (mol·cm^3/g^2 = cm^3/(g·daltons)) (g/mol = daltons) as

$$Hc/R(K) = 1/[M_w P(K)] + 2A_2 c + ... \qquad (19)$$

where $H = 4\pi^2 n^2 (\partial n/\partial c)_{T,P}^2 / N_A \lambda^4$ in usual notations. The specific refractive index increment of PBLG in DMF was taken to be 0.120 cm^3/g.[19b] $P(K)$ is expanded as $P(K)^{-1} = 1 + (1/3)\langle r_g^2\rangle_z K^2 + ...$ at sufficiently small K. We used Berry's method,[32] the plot of $P(K)^{-1/2}$ against K^2. At a finite concentration the slope and the intercept of $[Hc/R(K)]^{1/2}$ against K^2 give $\langle r_g(c)^2\rangle_z$.

The measured intensity autocorrelation function in the homodyne mode has the form of $G^2(\tau) = A[1 + \beta|g^1(\tau)|^2]$, where $g^1(\tau)$ is the normalized field correlation function, A is the base line, and β is a machine constant, which is determined in the data-fitting procedure. For $g^1(\tau)$, we adopted two forms. One is the cumulant expansion[33]

$$g^1(\tau) = \exp[-\bar{\Gamma}\tau + (\mu_2/2)\tau^2 - (\mu_3/6)\tau^3 + ...] \qquad (20)$$

where $\bar{\Gamma}$ is the average decay rate or the first cumulant and μ_2 is the second cumulant. $\mu_2/\bar{\Gamma}^2$ gives the normalized dispersion of the decay rate distribution. The other is the two-exponential fit. In the presence of polydispersity, however, a simple two-exponential fit does not give sufficiently precise results, and a modified equation can be used to retrieve the effect of polydispersity

$$g^1(\tau) = A_0 \exp[-\bar{\Gamma}_0\tau + (\mu_{2,0}/2)\tau^2] + A_2 \exp[-\bar{\Gamma}_2\tau + (\mu_{2,2}/2)\tau^2] \qquad (21)$$

where $\bar{\Gamma}_0$ (slow) and $\bar{\Gamma}_2$ (fast) are the decay rates of components with amplitudes A_0 and A_2, respectively. $\mu_{2,0}$ and $\mu_{2,2}$ are the corresponding second cumulants. At not very large K^2, $\bar{\Gamma}_0$ corresponds essentially to the contribution from translational diffusion and $\bar{\Gamma}_2$ from internal motions, such as rotational diffusion. In the case of rodlike polymers, as was discussed previously,[7] $\bar{\Gamma}_0/K^2$ has a weak K^2 dependence relating to the diffusion anisotropy. So, it is not unreasonable to assume $\bar{\Gamma}_0 = \langle D_0\rangle_z K^2$ and $\mu_{2,0}/\bar{\Gamma}_0^2 = \mu_2/\bar{\Gamma}^2$, which are obtained by the cumulant method at small K^2. By this, the number of unknowns to be determined can be reduced. At large K^2, $\bar{\Gamma}_2$ has the contribution of not only the first rotational diffusion mode but also higher rotational modes[34] and flexion modes. In order to obtain the rotational diffusion coefficient, the extrapolation of $(\bar{\Gamma}_2 - \bar{\Gamma}_0)/6$ to $K^2 = 0$ is necessary. From the analogy to a rod case,[7] this extrapolation is expected to give the rotational diffusion coefficient.

In the above methods of data analysis, goodness of the data fitting is monitored in several points. The reduced sum of squares of residuals to the fit, χ^2, should be reasonably small enough, the standard deviation of parameters determined should be less than 10%, and the deviation of the fitted correlation function from the measured one should be reasonably random over the entire delay time.

In all measurements, the sampling time ($\Delta\tau$), or the channel delay time, is chosen so that the total delay time, $240\Delta\tau$, is about $3/\bar{\Gamma}$ in order to ensure a high quality of data analysis. At small K^2 it was confirmed that the decrease of $\Delta\tau$ to, for example, one-third of the above value gave essentially the same $\bar{\Gamma}$ value.

Table I
Molecular Parameters of PBLG in DMF at 25 °C

parameter	PBLG-A	PBLG-B
$10^{-4}M_w$	29.9	37.2
10^4A_2, cm³/(g·daltons)	3.1	3.3
L_w, nm	205	255
$\langle r_g^2\rangle_z^{1/2}$, nm	57.5 (52.5)[a]	72.0 (63.6)[a]
$10^7\langle D_0\rangle_z$, cm²/s	1.36 (1.34)[b]	1.11 (1.13)[b]
k_D, cm³/g	17	18
Θ, s⁻¹	~3000 (3000)[c] (3060)[d]	~1800 (1800)[c] (1840)[d]
γL_w	0.655	0.815
$\mu_2/\bar{\Gamma}^2$	~0.20	~0.25
c[e]	0.10	0.11
ρ[f]	2.88	2.94

[a] By use of eq 24. [b] By use of Yamakawa–Fujii theory.[16] [c] By use of Yoshizaki–Yamakawa theory.[17] [d] By use of Hagerman–Zimm theory.,[30] [e] The C parameter defined in eq 18. [f] $\rho = \langle r_g^2\rangle_z^{1/2}\langle D_0\rangle_z/(k_BT/6\pi\eta)$. For calculation of theoretical values (a–d) $L = L_w$, $d = 2.2$ nm, and $\gamma^{-1} = 313$ nm were used.

At large K^2 the so chosen value of $\Delta\tau$ was so small, for example, $\Delta\tau = 0.5$ μs at the scattering angle of 150°, that the decrease of $\Delta\tau$ caused an accelerated after-pulse effect and a poor signal-to-noise ratio, and the accuracy of the data analysis became increasingly worse. Thus, the criterion of $240\Delta\tau\bar{\Gamma} \sim 3$ was maintained throughout.

By using $\bar{\Gamma}$ obtained as above, we can obtain another parameter characterizing the concentration dependence of the translational diffusion coefficient, $D_0(c) = D_0[1 + k_Dc + ...]$, where k_D is directly related to A_2 and k_f in $f(c) = f_0[1 + k_fc + ...]$ (concentration dependent friction factor), as

$$k_D + k_f = 2A_2M_w + \bar{v}_2 \quad (22)$$

where $\bar{v}_2$ is the partial specific volume of the polymer and is equal to 0.791 cm³/g for PBLG in DMF at 25 °C.[19] According to Itou et al.,[35] k_f in ref 36 is expressed with D_0 for a cylindrical rod as

$$k_f = (k_BT/3\eta)(3A_2N_A^{1/2}/2\pi)^{2/3}(M_w^{1/3}/D_0) \quad (23)$$

As k_f of a semiflexible chain has not been given, this equation provides a first-order approximation for PBLG in DMF.

Results and Discussion

1. Characterization of PBLG. The molecular parameters of PBLG samples determined by static and quasielastic light-scattering measurements are tabulated in Table I. The scattered intensity $Hc/R(0)$, the translational diffusion coefficient $\langle D_0(c)\rangle_z$, and the radius of gyration $\langle r_g(c)^2\rangle_z^{1/2}$ as functions of the concentration of PBLG-B are shown in Figure 2. The scattering function of PBLG-B is also shown in Figure 2c in $P(K)^{-1/2}$ vs. K^2. $\langle D_0\rangle_z$ was determined by the extrapolation of $\bar{\Gamma}/K^2$ to $c = 0$ and $K^2 = 0$. The rotational diffusion coefficient, Θ, was estimated from $(\bar{\Gamma}_2 - \bar{\Gamma}_0)/6$ of the two-exponential analysis of the correlation functions (for extrapolation to $K^2 = 0$, see discussion given below). The values of $\mu_2/\bar{\Gamma}^2$ determined at small K^2 are ~0.2 for PBLG-A and ~0.25 for PBLG-B.

By assuming 0.15 nm for the helical pitch per monomer units,[19,35] the molecular weight per unit contour length M_L is obtained to be 1460 daltons/nm. Then, the weight-average length L_w is calculated from M_w/M_L. The flexibility parameter γL_w is calculated by use of $\gamma^{-1} = 313$ nm from Yamakawa.[18,37] The diameter d is set to be 2.2 nm.[35] This d value is from sedimentation and dielectric studies and is slightly larger than that from viscometric measurements. This situation is observed in several other systems, for example, in poly(hexyl isocyanate).[38] Several previous works adopted a γ^{-1} value smaller than 313 nm.

By using these parameter values, we have calculated theoretical predictions of the radius of gyration and translational and rotational diffusion coefficients; these

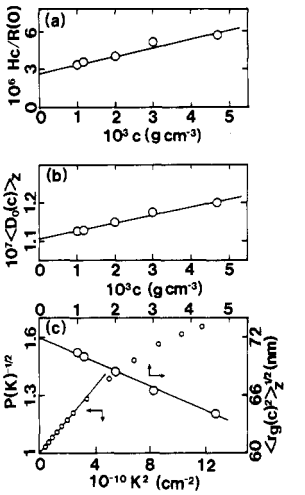

Figure 2. Concentration dependence of the static scattering intensity, the translational diffusion coefficient, and the radius of gyration of PBLG-B in DMF at 25 °C and the wavelength of the incident beam of 488.0 nm in vacuum. (a) Plot of $Hc/R(0)$ (in units of daltons⁻¹) as a function of concentration c. From this plot, $M_w = 3.72 \times 10^5$ and $A_2 = 3.3 \times 10^{-4}$ cm³/(g·daltons) were obtained. (b) Plot of $\langle D_0(c)\rangle_z$ (in units of cm²/s) as a function of c. $\langle D_0(c)\rangle_z$ was determined by an extrapolation of $\bar{\Gamma}/K^2$ at c to $K^2 = 0$. From this plot, $\langle D_0\rangle_z = 1.11 \times 10^{-7}$ cm²/s and $k_D = 18$ cm³/g were obtained. (c) Plot of $\langle r_g(c)^2\rangle_z^{1/2}$ as a function of c. In this figure, the scattering function is also plotted in $P(K)^{-1/2}$ vs. K^2, the initial slope of which gives $\langle r_g(c)^2\rangle_z$.

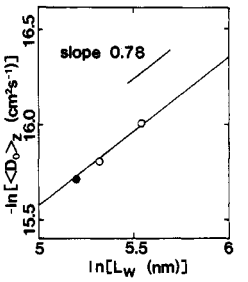

Figure 3. Double-logarithmic plot of $\langle D_0\rangle_z$ vs. L_w for PBLG in DMF at 25 °C. Hollow circles show the present results, and the filled circle is from the previous result.[14] The solid line shows the Yamakawa–Fujii theory[16] with $\gamma^{-1} = 313$ nm and $d = 2.2$ nm.

are also listed in Table I. Here, the radius of gyration of a wormlike chain is given by[39]

$$\langle r_g^2\rangle = \gamma^{-2}\{\gamma L/6 - \tfrac{1}{4} + 1/(4\gamma L) - [1 - \exp(-2\gamma L)]/[2(2\gamma L)^2]\} \quad (24)$$

with $L = L_w$; D_0 is given by Yamakawa–Fujii's theory[16] and Θ by the theories of Yoshizaki–Yamakawa[17] and Hagerman–Zimm.[30] Though D_0 and Θ show a close agreement with the measured ones, the radius of gyration shows a relatively large discrepancy. This indicates the effect of polydispersity. Since the radius of gyration is very sensitive to polydispersity, an effect of polydispersity has to be taken into account. This is discussed below together with the K^2 dependence of $\bar{\Gamma}/K^2$. On the other hand, since the effect of polydispersity on transport coefficients is expected to be less, the validity of adopted values of γ and d are examined against D_0 and Θ. For $\gamma^{-1} = 313$ and 180 nm,[14,40] and $d = 1.5$ nm,[40] 1.88 nm,[35] and 2.2 nm,[35] D_0 and Θ are calculated and listed in Table II. Comparing these values, we find that the combination of $\gamma^{-1} = 313$ nm and $d = 2.2$ nm gives the best agreement between experimental and computed values.

The theoretical prediction of D_0 by Yamakawa–Fujii's theory with $\gamma^{-1} = 313$ nm and $d = 2.2$ nm is shown in

Table II
Comparison of Diffusion Coefficients for Different Values of γ^{-1} and d

L_w, nm	γ^{-1}, nm	$10^7 D_0$,[a] cm^2/s			Θ,[b] s^{-1}		
		d = 1.5 nm	d = 1.88 nm	d = 2.2 nm	d = 1.5 nm	d = 1.88 nm	d = 2.2 nm
205	180	1.46	1.40	1.36	4270	4030	3860
					4340	4090	3910
	313	1.44	1.38	1.34	3310	3120	3000
					3390	3190	3060
255	180	1.24	1.19	1.15	2690	2540	2440
					2700	2550	2450
	313	1.21	1.16	1.13	1980	1870	1800
					2020	1910	1840

[a] By use of Yamakawa–Fujii theory.[16] [b] Upper values by use of Yoshizaki–Yamakawa theory;[17] lower values by use of Hagerman–Zimm theory.[30]

Figure 3, where the present experimental results are given together with the previous one for $M_w = 26.8 \times 10^4$.[14] The agreement is very good. However, the theoretical D_0 value is insensitive to γ^{-1} and d, and the present range of molecular weights is not wide enough to conclude that the combination of γ^{-1} = 313 nm and d = 2.2 nm is the most probable. The theoretical Θ value, on the other hand, is very sensitive to γ^{-1} and d, and our experimental Θ values favor the combination of γ^{-1} = 313 nm and d = 2.2 nm. (Since the statistical uncertainties in Θ values determined by the two-exponential analysis are not clear, the direct comparison of experimental Θ values with theoretical ones is a little hasty. As is discussed below, however, we have two more pieces of evidence to support the above combination of γ^{-1} and d values.)

Schmidt gave γ^{-1} = 140 nm by comparing the experimental $\langle r_g^2 \rangle_z$ with the predicted one for the assumed Schulz–Zimm distribution function. But, his samples had quite large values of M_w/M_n, and it was not clear whether the molecular weight distribution function was well approximated by the assumed function. Since the radius of gyration is very sensitive to polydispersity, the γ^{-1} value estimated in such a way is ambiguous, and it seems to be dangerous to use such a low γ^{-1} value for the present analysis.

The values of A_2 and k_D are quite comparable with other data.[23,35,41] When eq 22 is used, k_f is calculated to be 169 cm^3/g and 229 cm^3/g for PBLG-A and -B, respectively. These are compared with the calculated values (by use of eq 23 for a rigid rod) of 205 cm^3/g and 265 cm^3/g, respectively. The difference should be attributed partly to the contribution of flexibility, but since eq 23 is not sufficiently examined yet, we do not discuss further.

The ratio, ρ, of the radius of gyration to the apparent hydrodynamic radius defined by $\rho = \langle r_g^2 \rangle_z^{1/2} \langle D_0 \rangle_z / (k_B T / 6\pi\eta)$ is also listed in Table I. These are to be compared with the values calculated for the wormlike chains with L_w = 205 nm and 255 nm, that is, 2.59 and 2.64, respectively, from the values in parentheses in Table I. Discrepancies should be attributed to polydispersity of samples. Both experimental and computed values of the ratio was substantially larger than those predicted for Gaussian chains with the same contour lengths.

2. Two-Exponential Analysis. The two-exponential analysis for PGLB-A and -B by use of eq 21 gives $(\bar{\Gamma}_2 - \bar{\Gamma}_0)/6$ in Figure 4 and the amplitude ratio $A_2/(A_0 + A_2)$ in Figure 5. $\mu_{2,2}/\bar{\Gamma}_2^2$ is almost the same as $\mu_{2,0}/\bar{\Gamma}_0^2$ ($=\mu_2/\bar{\Gamma}^2$ at low K^2) at each K^2. The average decay rates defined by $\bar{\Gamma} = (A_0\bar{\Gamma}_0 + A_2\bar{\Gamma}_2)/(A_0 + A_2)$ from the two-exponential analysis give a good agreement with the results obtained by the cumulant method given below (Figure 6). $(\bar{\Gamma}_2 - \bar{\Gamma}_0)/6$ should give Θ at small K^2 where neither higher order rotational modes nor flexion modes contribute. But, because of smallness of $A_2/(A_0 + A_2)$ and remaining polydispersity effects, the two-exponential analysis did not give definitive results at small K^2. Although the data for K^2 dependence of $(\bar{\Gamma}_2 - \bar{\Gamma}_0)/6$ for PBLG-B show some scatter, $(\bar{\Gamma}_2 - \bar{\Gamma}_0)/6$ seems to be an increasing function of K^2. The extrapolated values of $(\bar{\Gamma}_2 - \bar{\Gamma}_0)/6$ to $K^2 = 0$ seem to be quite close to the values calculated by theories of Yoshizaki–Yamakawa[17] and Hagerman–Zimm.[30] The theoretical expression for $(\bar{\Gamma}_2 - \bar{\Gamma}_0)/6$ for a rigid rod has been given[7]

$$(\bar{\Gamma}_2 - \bar{\Gamma}_0)/6 = \Theta + (2/63)(D_3 - D_1)K^2 + (1/6)[2A_0(\mu^2) - A_2(\mu^2)](D_3 - D_1)^2K^4/\Theta \quad (25)$$

where $\mu^2 = (D_3 - D_1)K^2/\Theta$ and the explicit form of $A_n(\mu^2)$

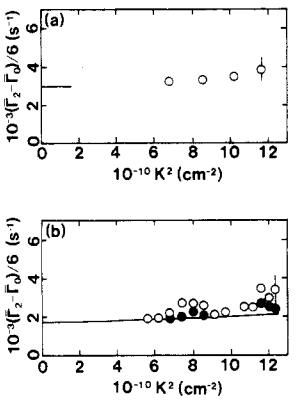

Figure 4. $(\bar{\Gamma}_2 - \bar{\Gamma}_0)/6$ vs. K^2 relationships for PBLG-A (a) and -B (b) at 25 °C. $\bar{\Gamma}_2$ is from a modified two-exponential analysis of correlation functions (eq 21). For $\bar{\Gamma}_0$, see text. The solid line in a shows the extrapolated value to $K^2 = 0$. The solid curve in b shows the predicted K^2 dependence of $(\bar{\Gamma}_2 - \bar{\Gamma}_0)/6$ (eq 25) for a rigid rod with $D_0 = 1.12 \times 10^{-7}$ cm^2/s, $\Theta = 1800$ s^{-1}, $(D_3 - D_1)/D_0 = 0.391$, and L = 255 nm. Filled circles show the results for given values of $A_2/(A_0 + A_2)$ of the dashed line in Figure 5b for comparison.

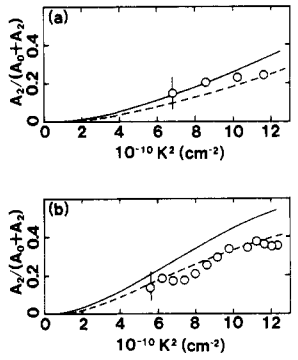

Figure 5. $A_2/(A_0 + A_2)$ vs. K^2 relationships for PBLG-A (a) and -B (b). A_0 and A_2 are from a modified two-exponential analysis of correlation functions (eq 21). The solid and dashed lines denote the predicted curves for a rigid rod in isotropic ($D_3 = D_1$) and anisotropic ($D_3 \neq D_1$) translation, respectively.

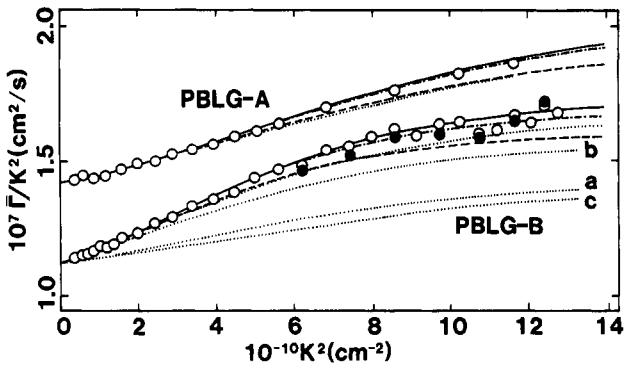

Figure 6. $\bar{\Gamma}/K^2$ vs. K^2 relationships for PBLG-A at 1.56 mg/mL and -B at 1.18 mg/mL at 25 °C. Hollow circles show the experimental results. Filled circles show some of the average decay rates for PBLG-B defined by $\bar{\Gamma} = (A_0\bar{\Gamma}_0 + A_2\bar{\Gamma}_2)/(A_0 + A_2)$ from the results in Figures 4 and 5. They show a little smaller but reasonable values compared with those of the cumulant analysis (hollow circles) if relatively large uncertainties in the two-exponential fit are taken into account. A little better fitting is observed for PBLG-A than PBLG-B (data not shown to avoid cluttering). The dotted lines show the predicted curves for rigid rods (eq 6). Dotted line a: anisotropic. Dotted line b: isotropic. Both are for the same D_0 and L as PBLG-B, and Θ and $(D_3 - D_1)/D_0$ are evaluated by use of Broersma's formulas. Dotted curve c: anisotropic and for an equivalent rod that gives the observed D_0 and Θ values for PBLG-B, i.e., L = 212 nm, d = 3.0 nm, and $(D_3 - D_1)/D_0$ = 0.470. Dotted line *without labels*: anisotropic and for parameter values for PBLG-A of $D_0 = 1.42 \times 10^{-7}$ cm²/s, Θ = 3000 s^{-1}, $(D_3 - D_1)/D_0$ = 0.413, γ^{-1} = 313 nm, d = 2.2 nm, and L = 205 nm, and for PBLG-B of $D_0 = 1.12 \times 10^{-7}$ cm²/s, Θ = 1800 s^{-1}, $(D_3 - D_1)/D_0$ = 0.391, γ^{-1} = 313 nm, d = 2.2 nm, and L = 255 nm. Dashed, dot–dash, and solid lines show the predicted curves for semiflexible filaments (eq 9) for the parameter values given above: dashed lines, without $a_n(k)$ terms; dot–dash lines, and $a_2(k)$ only; solid lines, with $a_2(k)$ and $a_3(k)$.

is found elsewhere.[7] The theoretical curve for a rigid rod with Θ = 1800 s^{-1} and $(D_3 - D_1)/D_0$ = 0.391 is shown in Figure 4b, which gives the first-order estimation of $(\bar{\Gamma}_2 - \bar{\Gamma}_0)/6$ for a semiflexible chain, and can be used as a good guideline for the extrapolation to $K^2 = 0$. As is seen in Figure 4b, the observed $(\bar{\Gamma}_2 - \bar{\Gamma}_0)/6$ deviates, from the line, upward with increasing K^2. This tendency has been observed for tobacco mosaic virus,[7] too, suggesting contributions from higher order rotational modes. Similarly to this, the upward deviation in the case of PBLG is interpreted to be due to the contribution from additional flexion modes. Even small amplitudes of such modes fairly affect the force-fitted values of $\bar{\Gamma}_2$.

In Figure 5, the fraction of the fast-decay component, $A_2/(A_0 + A_2)$, is shown as a function of K^2. Theoretical curves of the fraction for a rigid rod are also shown for cases of isotropic (—) and anisotropic (---) translation. For PBLG-A, experimental points of the fraction are between the solid and dashed curves. This is interpreted as a result of the decrease in anisotropy due to flexibility. For PBLG-B, experimental points of the fraction lie near, or a little lower than, the dashed curve. The lower values of the fraction have also been observed for tobacco mosaic virus,[7] when the force-fit to two exponentials was made for cases that higher order rotational modes contribute appreciably. As is shown below, the flexion modes contribute clearly to the correlation functions for PBLG-B at $K^2 \gtrsim 4 \times 10^{10}$ cm^{-2}, and this causes such deviation in the fraction.

3. Cumulant Analysis. The $\bar{\Gamma}/K^2$ vs. K^2 relationships for PBLG-A and -B are shown in Figure 6, where $\bar{\Gamma}$ was determined by the third-order-cumulant expansion of the correlation functions. From the initial slopes of these curves, the parameter C in eq 18 was determined to be 0.10 and 0.11 for PBLG-A and -B, respectively. These values are compared with the values reported by Schmidt.[23] Our C values were obtained for finite concentrations of PBLG. But, the difference of these values from those at the infinite dilution may be small; indeed, Schmidt observed no concentration dependence of C.[23]

We now examine the $\bar{\Gamma}/K^2$ vs. K^2 relationship in terms of flexibility with the aid of the formulation discussed in the theoretical section. In order to clarify the effect of flexibility on $\bar{\Gamma}/K^2$, we first study the behavior of theoretical $\bar{\Gamma}/K^2$ curves for a rigid rod with the same D_0 (= $\bar{\Gamma}/K^2$ at $K^2 = 0$) and L as PBLG-B. In Figure 6 are shown the theoretical $\bar{\Gamma}/K^2$ vs. K^2 for the rod in the presence (dotted curve a) and absence (dotted curve b) of anisotropy in translation. In these cases, the Θ value was calculated by use of Broersma's formula, and $(D_3 - D_1)/D_0$ = 0.5 (from Broersma's formulas), which was larger than 0.391 from eq 17 for a wormlike chain. Curve a underestimates $\bar{\Gamma}/K^2$ very much. Even curve b predicts substantially smaller $\bar{\Gamma}/K^2$ than the experimental one. This situation is quite similar to that observed before.[14] If we determine effective rod length and diameter so that D_0 and Θ from Broersma's formulas give the same values as the observed ones for PBLG-B, we obtain L = 212 nm, d = 3 nm, and $(D_3 - D_1)/D_0$ = 0.470. The theoretical $\bar{\Gamma}/K^2$ curve for these parameter values is also shown in Figure 6 by dotted curve c, and this is even below curve a. These curves (a and c) show large discrepancies from the experimental curve even at small K^2. This result implies that the light-scattering spectrum for PBLG-B cannot be explained by an effective equivalent rigid rod. As was considered above, the rigid-rod model cannot explain experimental results even qualitatively. This fact strongly suggests the importance of flexibility in the present results.

Next, by using the experimental values of D_0 and Θ and assuming $(D_3 - D_1)/D_0$ from eq 17, theoretical $\bar{\Gamma}/K^2$ curves for PBLG-A and -B are calculated with $f_1(k)$ and $f_2(k)$ for a rod. They are shown in Figure 6 by the dotted curve (without labels). The dotted curve (without label) for PBLG-B gives much smaller discrepancy from the experimental curve than any of the labeled dotted curves. But, systematic deviations are still observed, especially at large K^2, suggesting again the contribution from flexion modes. This means that even if all the transport coefficients are taken to be the same as those for PBLG samples, the scattering spectrum cannot be represented by the formulation for a rigid rod (eq 6).

Finally, eq 9 for a semiflexible filament is applied in order to analyze the $\bar{\Gamma}/K^2$ vs. K^2 relationship including the contribution of flexion modes. Both $f_1^*(k)$ and $f_2^*(k)$ are calculated for molecular parameters in Table I (see Figure 1 for PBLG-B). The theoretical $\bar{\Gamma}/K^2$ curves by use of eq 9 with $a_n(k) = 0$ are shown by dashed curves in Figure 6. These curves are not so different from the dotted curves (without labels) in each case, but a clear difference appears at large K^2 for PBLG-B. In these curves, the effect of flexibility is retrieved only through $I_{n,m}$ terms. The assumption of $a_n(k) = 0$ corresponds to the case that the amplitudes (the relaxation times) of flexion modes are too small (too short) to be detected in the experimental range of K^2. This can be checked by a criterion whether or not $\langle\delta_n^2\rangle^{1/2}$ (τ_n) is much smaller (shorter) than $1/K$ $(\Delta\tau)$, where $\langle\delta_n^2\rangle^{1/2}$ (τ_n) is the mean-square amplitude (the relaxation time) of the nth flexion mode.[11] $\langle\delta_2^2\rangle^{1/2}$ (τ_2) is calculated to be 12.7 nm and 16.7 nm (10.2 and 20.0 μs) for PBLG-A and -B, respectively, and $1/K$ $(\Delta\tau)$ is ~32 nm (0.8 μs), for example at the scattering angle of 120°. Then, the neglect of the flexion modes of at least n = 2 is not valid.

Therefore, the theoretical $\bar{\Gamma}/K^2$ values including $a_2(k)$ are calculated and shown in Figure 6 by the dot-dahsed curves. The agreement of these curves with the experimental results becomes much better, and theoretical curves predict almost quantitatively the K^2 dependence of $\bar{\Gamma}/K^2$ over all K^2, indicating the important contribution of the $n = 2$ mode. Especially for PBLG-B, the contribution of the $n = 2$ mode is noticeable even at relatively small K^2, $K^2 \sim 4 \times 10^{10}$ cm^{-2}. Moreover, the theoretical $\bar{\Gamma}/K^2$ curves including $a_2(k)$ and $a_3(k)$ are also shown in Figure 6 by the solid curves. The contribution of the $n = 3$ mode is quite small for PBLG-A and only a little greater at large K^2 for PBLG-B. When the contribution of flexion motion is explicitly included, the behavior of the experimental $\bar{\Gamma}/K^2$ as a function of K^2 is well described, and it is clear that flexibility plays an important role in the light-scattering spectrum of PBLG-A and -B.

The effect of hydrodynamic interaction on $\bar{\Gamma}/K^2$ was previously examined for fd virus for which γL was 0.23. Even for this small value of γL, the hydrodynamic interaction definitely affected the theoretical results, and the explicit inclusion of this interaction was important for a quantitative determination of the γL values. For PBLG, f_n is not small; $f_2 = 2.56$ for PBLG-A, and $f_2 = 2.98$ for PBLG-B. The hydrodynamic interaction is important in estimating the contribution of flexion modes to $\bar{\Gamma}/K^2$ for PBLG samples, too.

4. Some Remarks. a. On Dilute Regime. For PBLG samples used in this experiment, cL^3 (c: the number concentration) for 1 mg/mL is ~17 (PBLG-A) and ~27 (PBLG-B). When the concentration of PBLG is lowered to access the condition $cL^3 < 1$ for dilute regime, the scattered intensity is too weak to be detected and analyzed properly, and it is almost impossible to obtain definitive results. Zero and Pecora, however, reported that the rotational diffusion coefficient started to decrease at $cL^3 \sim 50$, where the actual onset of the semidilute region appeared to occur.[42] Thus, our concentrations of PBLG, 1.56 mg/mL for PBLG-A and 1.18 mg/mL for PBLG-B (both in Figure 6), are considered to be within the dilute regime, and our discussion given in section 3 based on the formulation for dilute regime is approved.

b. On Transport Coefficients. Theoretical calculations presented here premise many points and are approximate. It is necessary to examine the validity of each term in eq 9 in more detail. Yamakawa–Fujii's theory for D_0 predicted experimental results for PBLG very well if $\gamma^{-1} = 313$ nm and $d = 2.2$ nm were assumed (Figure 3). Although $d = 2.2$ nm is much larger than the geometric diameter of 1.5 nm in the crystalline state, the former value should be regarded as a hydrodynamically effective one. For the same γ^{-1} and d values as above, theories by both Yoshizaki–Yamakawa and Hagerman–Zimm gave Θ values very close to each other and to our experimental results. Furthermore, we observed that these theories could predict very well the experimental Θ values for DNA by Elias and Eden[43] if the rise per base pair and the diameter were set to be 0.34 nm and 2.7 nm, respectively. These values are quite reasonable. Although an experimental examination of the validity is very difficult, it is probable that eq 17 is highly approximate and will underestimate $(D_3 - D_1)/D_0$ for γL of the present interest. If this is the case, the dashed curves in Figure 6 overestimate $\bar{\Gamma}/K^2$. It should be mentioned that if anisotropy in translation is ignored, the dashed curves in Figure 6 shift upward largely beyond the experimental points for both PBLG-A and -B. This suggests the important contribution to $\bar{\Gamma}/K^2$ from anisotropy in translation.

c. Effect of Polydispersity. The present PBLG samples have some degree of polydispersity, though it is expected to be relatively narrow. We try to estimate the effect of the length distribution on the spectrum for an assumed distribution function, i.e., a Schulz–Zimm distribution function. The weight fraction of the chain with contour length L, $W(L)$, is given by[44]

$$W(L)\,dL = [(m+1)^{m+1}/\Gamma(m+1)] \times (L/L_w)^m \exp[-(m+1)L/L_w]\,d(L/L_w) \quad (26)$$

where m is the distribution parameter and $\Gamma(m+1) = m\Gamma(m)$ is the Γ function, which equals $m!$ for integers m. The monodisperse distribution is given by $m = \infty$.

From eq 24 and 26, we have[23]

$$\langle r_g^2\rangle_z = \gamma^{-2}\left\{\frac{m+2}{m+1}\frac{\gamma L_w}{6} - \frac{1}{4} + \frac{1}{4\gamma L_w} - \frac{m+1}{m}\left[1 - \left(1 + \frac{2\gamma L_w}{m+1}\right)^{-m}\right]/[2(2\gamma L_w)^2]\right\} \quad (27)$$

With $\gamma^{-1} = 313$ nm, we obtain $\langle r_g^2\rangle_z = (57.5\text{ nm})^2$ for $m = 11$ and $L_w = 205$ nm and of $(72.0\text{ nm})^2$ for $m = 7.2$ and $L_w = 255$ nm. With $\gamma^{-1} = 180$ nm, on the other hand, we obtain $\langle r_g^2\rangle_z$ of $(57.5\text{ nm})^2$ for $m = 4.3$ and $L_w = 205$ nm and of $(72.0\text{ nm})^2$ for $m = 2.7$ and $L_w = 255$ nm. Which set of parameter values is more plausible in our PBLG samples? For this purpose, we now introduce another criterion. From eq 26, we have $L_w/L_n = M_w/M_n = (m+1)/m$, where L_n and M_n are the number-average contour length and molecular weight, respectively. For a rigid rod, we have $M_w/M_n \sim 1 + \mu_2/\bar{\Gamma}^2$ (ref 14). From the experimental values of $\mu_2/\bar{\Gamma}^2$ at low angles, we obtain $M_w/M_n \sim 1.2$ or $m \sim 5$ for PBLG-A and $M_w/M_n \sim 1.25$ or $m \sim 4$ for PBLG-B. The $\mu_2/\bar{\Gamma}^2$ is very sensitive to dusts in the scattering samples and noise in the correlation functions. In addition, for PBLG-B, $\bar{\Gamma}/K^2$ at $K^2 \sim 1 \times 10^{10}$ cm^{-2} substantially increases from the value at $K^2 \to 0$, indicating the contribution of the rotational (and/or flexion) mode. This contribution also causes an increase in $\mu_2/\bar{\Gamma}^2$; that is, $\mu_2/\bar{\Gamma}^2$ is usually larger than that coming from the molecular weight distribution alone. Then the above estimates of m from $\mu_2/\bar{\Gamma}^2$ should be regarded as lower bounds. These considerations favor $m = 11 - 7$ and $\gamma^{-1} = 313$ nm compared with $m = 4 - 3$ and $\gamma^{-1} = 180$ nm. In the following we assume $m = 8$ for our PBLG samples.

For $L_w = 255$ nm, $d = 2.2$ nm, and $\gamma^{-1} = 313$ nm, the Yamakawa–Fujii theory[16] and eq 26 give $D_0 = 1.13 \times 10^{-7}$ cm^2/s ($m = \infty$, monodisperse) and $\langle D_0\rangle_z = 1.12 \times 10^{-7}$ cm^2/s ($m = 8$, polydisperse). Because of experimental errors and/or uncertainties in the determination of $\bar{\Gamma}/K^2$, this difference is unable to be detected. As was discussed by Schmidt,[23] the influence of polydispersity on the translational diffusion coefficient is very small when the weight-average length is used for its estimation.

Now we examine the effect of the length distribution on the spectrum for a rod system. This is based on the following considerations: At small K^2, the spectrum for a semiflexible chain is not so different from that for a rod. At large K^2, on the other hand, the increase in $\bar{\Gamma}/K^2$ for a rod, due to polydispersity, would give an upper bound of that for a semiflexible chain, since the scattering function for a rod decreases more rapidly than that for a semiflexible chain with increasing KL. And, theoretical formulas for the scattering function and for $\bar{\Gamma}/K^2$ (eq 6 or 28 just below) for a rigid rod are exactly known, so that the profile of $\bar{\Gamma}/K^2$ is easily calculated. By taking the above estimate of $m = 8$, the effect of polydispersity on

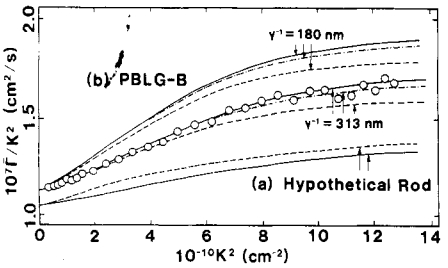

Figure 7. $\bar{\Gamma}/K^2$ vs. K^2 relationships. (a) Simulation of $\bar{\Gamma}/K^2$ for a hypothetical rod with polydispersity of a Schulz–Zimm distribution function. Solid and dashed lines denote the predicted curves for L_w = 250 nm, d = 2.2 nm, and m = ∞ and 8, respectively. The algorithm for calculation is quite similar to that in ref 45. (b) Simulation of $\bar{\Gamma}/K^2$ by use of eq 9 for γ^{-1} = 180 and 313 nm. Other parameter values are L = 255 nm and d = 2.2 nm. Dashed lines: without $a_n(k)$ terms. Dot–dash lines: with $a_2(k)$ only. Solid lines: with $a_2(k)$ and $a_3(k)$. Experimental points and theoretical lines for γ^{-1} = 313 nm are from Figure 6 (PBLG-B).

the $\bar{\Gamma}/K^2$ vs. K^2 relationship for a rigid rod is examined, and the result is shown in Figure 7a for L_w = 250 nm and d = 2.2 nm, where diffusion coefficients are calculated by use of Broersma's formulas for PBLG-B at 25 °C. Equation 6 can be written as

$$\bar{\Gamma}/K^2 = D_0 + (L^2/12)\Theta f_1(k) - (D_3 - D_1)[1/3 - f_2(k)] \quad (28)$$

Since both functions $f_1(k)$ and $[1/3 - f_2(k)]$ start from zero at $K^2 = 0$ and monotonically increase with K^2 (see Figure 1) and since $(D_3 - D_1)$ is positive, the effect of polydispersity on the second and the third terms in eq 30 almost cancel out each other, and the difference between the solid and the dashed curves in Figure 7a mostly comes from the difference between D_0 and K^2-dependent $\langle D_0 \rangle_z$.[45] Broersma's formula gives $D_0 = 1.06 \times 10^{-7}$ cm²/s (m = ∞) and $\langle D_0 \rangle_z = 1.05 \times 10^{-7}$ cm²/s at $K^2 = 0$ (m = 8), and the difference between these two values is again quite small as in the case of a wormlike chain given above. As for the K^2 dependence of $\bar{\Gamma}/K^2$, we have at $K^2 = 8.2 \times 10^{10}$ cm^{-2}, for example, $\bar{\Gamma}/K^2 = 1.28 \times 10^{-7}$ cm²/s (m = ∞) and 1.32×10^{-7} cm²/s (m = 8). The difference is only 3%. It should be noted again that the size of the increase in $\bar{\Gamma}/K^2$ for a rod, due to polydispersity, is expected to be an upper bound of that for a semiflexible chain (at least for eq 9 without $a_n(k)$ terms) and that the size in the increase in $\bar{\Gamma}/K^2$ for a rod is almost constant above $K^2 = 2 \times 10^{10}$ cm^{-2}, whereas the size in the difference between the experimental point and the dashed curve in Figure 6 is an increasing function of K^2 for both PBLG-A and -B. Another thing to be noted is that the theoretical $\bar{\Gamma}/K^2$ in eq 6 and 9 is for the slope at "τ = 0" of the correlation function, whereas the experimental $\bar{\Gamma}/K^2$ is for the slope of the correlation function at the finite channel width ($\Delta\tau$) of the digital correlator. Although a cumulant expansion more or less recovers the reduction in the experimental $\bar{\Gamma}/K^2$ values, they might be appreciably smaller than those at "$\Delta\tau$ = 0". Then it is likely that the difference at large K^2 between experimental points and theoretical dashed curves in Figure 6 largely exceeds the size of ambiguity coming from polydispersity, and the comparison of the experimental $\bar{\Gamma}/K^2$ vs. K^2 relationship with the theoretical one for the monodisperse preparation is quite meaningful. Strictly speaking, however, our examination given above is still semiquantitative and is opened for reevaluation in a more quantitative manner.

d. On Smaller Persistence Length. Although not conclusive, our experimental Θ values favor γ^{-1} = 313 nm. The examination of $\langle r_g^2 \rangle_z$ given above also favors γ^{-1} = 313 nm and m = 8 compared with γ^{-1} = 180 nm and m = 3. In Figure 7b are compared the theoretical $\bar{\Gamma}/K^2$ for γ^{-1} = 180 nm with those for γ^{-1} = 313 nm. The dashed curve for γ^{-1} = 180 nm tremendously overestimates the experimental $\bar{\Gamma}/K^2$. This came mainly from a larger Θ value for γ^{-1} = 180 nm (Θ = 2440 s^{-1}) than for γ^{-1} = 313 nm (Θ = 1800 s^{-1}). In addition, $f_1^*(k)$ [$f_2^*(k)$] for γ^{-1} = 180 nm is slightly smaller [larger] than for γ^{-1} = 313 nm. Thus, a smaller diffusion anisotropy at γ^{-1} = 180 nm than at 313 nm also increases the $\bar{\Gamma}/K^2$ value. This result again favors γ^{-1} = 313 nm compared with γ^{-1} = 180 nm.

e. Comparison with Earlier Results. Kubota and Chu studied PBLG ($M_w = 2.68 \times 10^5$) in DMF at 25 °C.[14] By a histogram analysis of correlation function at $K^2 = 11.6 \times 10^{10}$ cm^{-2} (135°), they obtained the rotational diffusion coefficient of Θ_h = 8330 s^{-1}. This value is expected to be influenced by contributions from higher order modes. Indeed, our results at the same K^2 give ~3900 s^{-1} (PBLG-A) and ~3500 s^{-1} (PBLG-B) (see Figure 4). They are 30% and 90% larger than those extrapolated to K^2 = 0, i.e., ~3000 s^{-1} (PBLG-A) and ~1800 s^{-1} (PBLG-B), respectively. The above Θ_h value is inferred to be 20~30% larger than at K^2 = 0, i.e., Θ_h = 8330/(1.2~1.3) = (6900~6400) s^{-1}. These corrected values are still larger than the theoretical prediction of Θ_{HZ} = 4960 s^{-1} (γ^{-1} = 180 nm) or Θ_{HZ} = 3950 s^{-1} (γ^{-1} = 313 nm) from Hagerman–Zimm's formula. This discrepancy is not clear.

Kubota and Chu also analyzed the experimental $\bar{\Gamma}$ vs. K^2 relationship with the aid of Maeda–Fujime's old model,[9] where neither anisotropy in translation nor the hydrodynamic interaction was taken into account. This theory gives the relaxation time τ_1 of the lowest flexion mode as

$$3(k_BT/\zeta L)\tau_1/L^2 = f(\gamma,L) \quad (29)$$

where $f(\gamma,L)$ is a function of γ and L and its explicit form is given elsewhere.[9] To take account of the hydrodynamic interaction semiquantitatively, Maeda and Fujime put $(k_BT/\zeta L) = D_1 = (3/4)D_0$ and suggested using experimental D_0 value for estimating τ_1. According to this protocol, Kubota and Chu obtained a good agreement between experimental and theoretical $\bar{\Gamma}$ vs. K^2 relationships (Figure 16 in ref 14). Since $\tau_1 = (3\Theta)^{-1}$, they estimated Θ_F = 7220 s^{-1}. This Θ_F value is much larger than Θ_{HZ} given above. However, this discrepancy can be reduced as follows.[11] To put $(k_BT/\zeta L) = D_1$ is equivalent to $(k_BT/\zeta L)(1 + f_0)$. To estimate τ_1, however, $(k_BT/\zeta L)$ in eq 29 should be replaced with $(k_BT/\zeta L)(1 + f_1)$. Indeed, we have $(12k_BT/\zeta L^3)(1 + f_1) = \Theta_{rod}$, and Θ(semiflexible) = $\Theta_{rod}/[12f(\gamma,L)]$. Here f_0 and f_1 are given by eq 16 for n = 0 and 1, respectively. To take account of the hydrodynamic interaction more quantitatively, τ_1^{KC} in Kubota and Chu should be corrected as $\tau_1 = \tau_1^{KC}/[(1 + f_1)/(1 + f_0)]$, or $\Theta_F = \Theta_F^{KC}(1 + f_1)/(1 + f_0)$. For d = 2.2 nm we have $(1 + f_0)/(1 + f_1) = 5.1/3.7 = 1.38$ (ref 11). Then, we have $\Theta_F = 7220/1.38 = 5230$ s^{-1} for γ^{-1} = 180 nm (Kubota and Chu adopted γ^{-1} = 180 nm). This corrected Θ_F should be compared with Θ_{HZ} = 4960 s^{-1} for γ^{-1} = 180 nm. The value of $f(\gamma,L)$ for γ^{-1} = 313 nm is 1.23 times larger than that for γ^{-1} = 180 nm. Then, similar to the above procedure for correction, we have $\Theta_F = 5230/1.23 = 4250$ s^{-1} for γ^{-1} = 313 nm. The Θ_F value should be compared with Θ_{HZ} = 3950 s^{-1} for γ^{-1} = 313 nm. Another thing to be noted is that the γL value in the old model[9] should be multiplied by 2/3 if compared with the γL value in the new model;[10-12] that is, γL = 1.0 (γ^{-1} = 180 nm) in Kubota and Chu corresponds to γL = 0.667 (γ^{-1} = 280 nm). From these "corrected" values alone it is difficult to conclude which γ^{-1} value is more likely, γ^{-1} = 180 or 313 nm. However, it must be mentioned that in Kubota and Chu only the l = 2 term of the τ_1 mode was considered.

$$G^1(\tau) = \exp(-D_0K^2\tau) \sum_{l:\text{even}} P_l(k) \exp[-(l/\tau_1)\tau] \sim P_0(k) \exp(-D_0K^2\tau) + P_2(k) \exp[-(D_0K^2 + 2/\tau_1)\tau] \quad (30)$$

Therefore, their simulation of the $\bar{\Gamma}$ vs. K^2 relationship required a smaller γ^{-1} value (a larger flexibility) than the true one. Indeed, our reanalysis based on eq 9 showed a little underestimation (a little overestimation) of the $\bar{\Gamma}$ vs. K^2 relationship for γ^{-1} = 313 nm (γ^{-1} = 180 nm).

Conclusions

We have measured the static and quasielastic light-scattering spectra for two samples of PBLG with different molecular weights in DMF at 25 °C. When both results were combined, various molecular parameters were determined. The experimental values of these parameters were reasonably predicted by recent theories if the values of γ^{-1} = 313 nm and d = 2.2 nm of Yamakawa were assumed. The analysis of quasielastic light-scattering spectrum by a modified two-exponential fit and by a cumulant expansion showed the important contribution of the chain flexibility and of anisotropy in translational diffusion. An explicit consideration of flexion modes with the hydrodynamic interaction gave a reasonable prediction about the observed $\bar{\Gamma}/K^2$ vs. K^2 relationship if γ^{-1} = 313 nm was again assumed. Any smaller γ^{-1} value used gave overestimation of Θ (and D_0) as well as of $\bar{\Gamma}/K^2$. Evaluation of $\bar{\Gamma}/K^2$ in eq 9 required many approximations, but it provided a good estimation for characterizing the dynamic behavior of a semiflexible chain by quasielastic light scattering.

Acknowledgment. We thank Professor K. Ogino of the University of Tokyo for the kind gift of the PBLG sample and Professor A. Kitahara of the Science University of Tokyo for permission to use his argon ion laser. This work was partly supported by a Grant-in-Aid from the Ministry of Education, Science, and Culture of Japan.

Registry No. PBLG (homopolymer), 25014-27-1; PBLG (SRU), 25038-53-3.

References and Notes

(1) Chu, B. *Laser Light Scattering*; Academic: New York, 1974.
(2) Berne, B.; Pecora, R. *Dynamic Light Scattering*; Interscience: New York, 1975.
(3) de Gennes, P.-G. *Scaling Concepts in Polymers Physics*; Cornell University: Ithaca, NY, 1979.
(4) The following are informative: (a) *Scattering Techniques Applied to Supramolecular and Nonequilibrium Systems*; Chen, S.-H., Chu, B., Nossal, R., Eds.; Plenum: New York, 1981. (b) *Biomedical Application of Laser Light Scattering*; Sattelle, D. B., Lee, W. I., Ware, B. R., Eds.; Elsevier Biomedical: Amsterdam and Oxford, 1982. (c) *The Application of Laser Light Scattering to the Study of Biological Motion*; Earnshaw, J. C., Steer, M. W., Eds.; Plenum: New York, 1983. (d) *Physical Optics of Dynamic Phenomena and Processing in Macromolecular Systems*; Sedlacek, B., Ed.; Walter de Gruyter: Berlin and New York, 1985.
(5) Maeda, H.; Saito, N. *J. Phys. Soc. Jpn.* **1969**, *27*, 984.
(6) Wilcoxon, J.; Schurr, J. M. *Biopolymers* **1983**, *22*, 849.
(7) Kubota, K.; Urabe, H.; Tominaga, Y.; Fujime, S. *Macromolecules* **1984**, *17*, 2096.
(8) Sharp, P.; Bloomfield, V. A. *Biopolymers* **1968**, *6*,1201.
(9) Maeda, T.; Fujime, S. *Macromolecules* **1981**, *14*, 809.
(10) Maeda, T.; Fujime, S. *Macromolecules* **1984**, *17*, 2381.
(11) Fujime, S.; Maeda, T. *Macromolecules* **1985**, *18*, 191.
(12) Maeda, T.; Fujime, S. *Macromolecules* **1985**, *18*, 2430.
(13) Kratky, O.; Porod, G. *Recl. Trav. Chim. Pays-Bas* **1949**, *68*, 1106.
(14) Kubota, K.; Chu, B. *Biopolymers* **1983**, *22*, 1461.
(15) Yamakawa, H.; Fujii, M. *Macromolecules* **1974**, *7*, 649.
(16) Yamakawa, H.; Fujii, M. *Macromolecules* **1973**, *6*, 407.
(17) Yoshizaki, T.; Yamakawa, H. *J. Chem. Phys.* **1984**, *81*, 982.
(18) Yamakawa, H. *Annu. Rev. Phys. Chem.* **1984**, *35*, 23.
(19) (a) Fujita, H.; Teramoto, A.; Yamashita, T.; Okita, K.; Ikebe, S. *Biopolymers* **1966**, *4*, 781. (b) Fujita, H.; Teramoto, A.; Okita, K.; Yamashita, T.; Ikebe, S. *Biopolymers* **1966**, *4*, 769.
(20) Budd, P. M.; Heatley, F.; Holton, T. J.; Price, C. *J. Chem. Soc., Faraday Trans. 1* **1981**, *77* 759.
(21) Schmidt, M.; Stockmayer, W. H. *Macromolecules* **1984**, *17*, 509.
(22) Burchard, W. *Adv. Polym. Sci.* **1983**, *48*, 1.
(23) Schmidt, M. *Macromolecules* **1984**, *17*, 553.
(24) Maeda, T.; Fujime, S. *Macromolecules* **1984**, *17*, 1157.
(25) Hearst, J. E.; Stockmayer, W. H. *J. Chem. Phys.* **1962**, *37*, 1425.
(26) Stockmayer, W. H.; Burchard, W. *J. Chem. Phys.* **1979**, *70*, 3138.
(27) Broersma, S. J. *J. Chem. Phys.* **1960**, *32*, 1625.
(28) Broersma's revised end-effect corrections are found in Newman, J.; Swinney, H. L.; Day, L. A. *J. Mol. Biol.* **1977**, *116*, 593.
(29) Tirado, M.; Garcia de la Torre, J. *J. Chem. Phys.* **1979**, *71*, 2581.
(30) Hagerman, P. J.; Zimm, B. H. *Biopolymers* **1981**, *20*, 1481.
(31) Nose, T.; Chu, B. *Macromolecules* **1979**, *12*, 590.
(32) Berry, G. C. *J. Chem. Phys.* **1966**, *44*, 4550.
(33) Koppel, D. E. *J. Chem. Phys.* **1972**, *57*, 4814.
(34) In $G^1(\tau) = \exp(-D_0K^2\tau)\sum_n S_n(k) \exp[-n(n+1)\Theta\tau]$ for $D_3 = D_1$ or in the corresponding expression for $D_3 \neq D_1$, we assign n = 2 for the first rotational mode and $n \geq 4$ for higher rotational modes.
(35) Itou, S.; Nishioka, N.; Norisuye, T.; Teramoto, A. *Macromolecules* **1981**, *14*, 904.
(36) Peterson, J. M. *J. Chem. Phys.* **1964**, *40*, 2680.
(37) Yamakawa, H.; Fujii, M. *J. Chem. Phys.* **1984**, *81*, 997.
(38) Murakami, H.; Norisuye, T.; Fujita, H. *Macromolecules* **1980**, *13*, 345.
(39) Benoit, H.; Doty, P. *J. Phys. Chem.* **1953**, *57*, 958.
(40) Moha, P.; Weill, G.; Benoit, J. *J. Chem. Phys.* **1964**, *61*, 1240.
(41) Russo, P. S.; Karasz, F. E.; Langley, K. H. *J. Chem. Phys.* **1984**, *80*, 5312.
(42) Zero, K.; Pecora, R. *Macromolecules* **1982**, *15*, 87.
(43) Elias, J. G.; Eden, D. *Macromolecules* **1981**, *40*, 410.
(44) Zimm, B. H. *J. Chem. Phys.* **1948**, *16*, 1099.
(45) Kubota, K.; Tominaga, Y.; Fujime, S.; Otomo, J.; Ikegami, A. *Biophys. Chem.* **1985**, *23*, 15.